Catalytic coating of virus particles with zinc oxide

S. Balci [a], A.M. Bittner [a,*], M. Schirra [b], K. Thonke [b], R. Sauer [b], K. Hahn [c], A. Kadri [d], C. Wege [d], H. Jeske [d], K. Kern [a,e]

[a] Max-Planck-Institut für Festkörperforschung, Heisenbergstr. 1, D-70569 Stuttgart, Germany
[b] Institut für Halbleiterphysik, Universität Ulm, D-89069 Ulm, Germany
[c] Max-Planck-Institut für Metallforschung, Heisenbergstr. 3, D-70569 Stuttgart, Germany
[d] Biologisches Institut, Pfaffenwaldring 57, D-70550 Stuttgart, Germany
[e] Institut du Physique des Nanostructures, Ecole Polytechnique Federale, CH-1015 Lausanne, Switzerland

ABSTRACT

We show that the rod-shaped *Tobacco mosaic virus* (TMV) can be coated with the wide band gap semiconductor zinc oxide by electroless deposition under mild reaction conditions. The process involves pretreatment with aqueous Pd(II), followed by nucleation of ZnO, directed to palladium centers formed on the surface of TMV. The mechanism is based on the local pH change due to the reduction of nitrate by dimethylamine borane at the palladium. Morphology and chemical composition have been analyzed by transmission electron microscopy (TEM) and by energy filtering TEM, respectively. The optical properties were elucidated by cathodoluminescence, which showed the desired near-band edge emission.

© 2009 Elsevier Ltd. All rights reserved.

1. Introduction

There is considerable interest in the synthesis of semiconducting nanowires with controlled dimension and morphology, which will be critical for the fabrication of electronic and photonic nanodevices [1]. Zinc oxide (ZnO) is a very promising semiconductor material for optical and electronic applications. For example, it has recently attracted increasing attention as a room-temperature ultraviolet light-emitting material because of its wide band gap energy of 3.37 eV and high exciton binding energy of ∼60 meV, which ensures that excitonic emission mechanisms are significant only at temperatures well above room temperature [2] (thermal energy 26 meV), suggesting that the electron–hole pairs are exceptionally stable. This might be an advantage in the development of efficient UV light emitting diodes. Small diameter ZnO nanowires are expected to further lower the laser emission threshold since quantum effects result in the enhancement of the density of states near the band edges, and in the radiative recombination due to carrier confinement [3]. For example, Huang et al. have reported a novel synthesis method for ZnO nanowires by a vapor transport and condensation process [2]. The wires grow selectively below Au catalyst particles attached to sapphire substrates because the ZnO precursor dissolves in the gold catalyst and segregates epitaxially.

Alternatively, electroless deposition routes can be applied for the synthesis of ZnO nanostructures; no electrical connection is required. Electrochemical strategies offer numerous advantages like being environmentally friendly, simple setup, low energy consumption, etc. Consequently, it becomes possible to integrate biomolecules in the process, which can be advantageous [4]. For example, a variety of morphologies have been observed by combining amino acids and peptides with Zn(II) salts [4]. Rod-like virus particles (virions) are attractive 1D templates [5–9] and should provide suitable scaffolds for ZnO nanowires. An especially promising candidate is *Tobacco mosaic virus* (TMV), which is 300 nm long and 18 nm in diameter [10]. The exactly known chemical and structural details allow for selective covalent linking or localized chemical reactions with metal ions [5–8] to give nanowires and linearly assembled nanostructures. TMV particles can aggregate end-to-end to form rods longer than single TMVs [11], especially in the presence of Cd(II) and Zn(II) [11], hence ZnO rods of up to some μm lengths can be expected.

ZnO can be produced from Zn(II) by electroless deposition (ELD; "chemical" deposition) (and also by galvanic or electrodeposition) [12,13]. Note that here ELD does not refer to the reduction of a metal cation, but merely to the presence of a reductant. The principle can be compared with the electrochemical deposition of oxides, where a reduction process creates a high local concentration of hydroxide.

However, the ELD mechanism of ZnO deposition is not yet completely understood. Izaki et al. have developed an ELD method for crystalline particulate ZnO films on Pd/Sn-sensitized glass [13,14]: Immersion in an aqueous solution of $Zn(NO_3)_2$ and dimethylamine borane (DMAB) at 50 °C [13]. The films show a characteristic band gap energy of 3.3 eV. In the same way, Saito and co-workers have demonstrated the fabrication of ZnO micropatterns by selective ELD of ZnO on silicon oxide [14]. The structures were probed by spatially resolved cathodoluminescence (CL). Here we describe a similar process that involves a soft, but well defined substrate, the outer surface of TMV. For sensitization, we employed pure Pd(II), followed by ELD of $Zn(NO_3)_2$ with DMAB. In this way the growth of ZnO rods can be achieved even at ambient temperature. Apart from a structural, chemical and optical analysis of single rods on the nanoscale, we employed dyes to elucidate the electrochemical mechanism of the process.

2. Experimental

For sensitization of TMV, we used Pd(II), as reported in ref [7]. Note that we avoided phosphate in most experiments, which has to be present for metallizations of the (exterior) surface of TMV. Electroless deposition (ELD) of ZnO films is supposed to proceed through the reduction of nitrate ions with dimethylamine borane (DMAB) [12,13]. We initially tested comparatively high concentrations of $Zn(NO_3)_2$ (0.05 M), but due to the high deposition rate we were unable to detect any TMV particles by TEM; presumably, all TMV particles were embedded in large ZnO agglomerates. Smaller concentrations of DMAB helped to optimize the deposition rate of ZnO, and a bath with 0.013 M $Zn(NO_3)_2$ and 0.05 M DMAB was found suitable. It is obvious that the concentration decrease of one of the educts, here Zn(II), is sufficient to decrease the growth rate of ZnO [15]. After 30 min, aliquots were taken for TEM and AFM analysis.

In contrast to the autocatalytic ELD of metals, our product, ZnO, is not a catalyst: After addition of DMAB to the $Zn(NO_3)_2$ solution, a small amount of white precipitate was observed, ZnO produced by pH changes of the solution (the DMAB is protonated). Its amount did not increase, so obviously the precipitate is not catalytically active. However, we filtered the bath before mixing it with the sensitized virion suspension to avoid such spontaneously produced ZnO.

Fig. 1 shows a TEM micrograph of ZnO-coated virions adsorbed on a TEM grid; AFM images are provided in the Supp. Info. The diameters of the ZnO rods are between 100 and 150 nm, and the lengths of the structures reach a few micrometers, depending on the length of the end-to-end assembled virions [11], which is in

turn increased by the presence of Zn(II). TMV particles (lighter shade) within ZnO rods can be discerned (see Fig. 1b). The rods are not completely smooth but granular (size ~100 nm). In contrast to metal ELD, removing the phosphate buffer in the TMV suspension by dialysis did not change the deposition behavior [6]. It is likely that the functional groups on the exterior virion coat, carboxylate, hydroxyl, and probably amine, facilitate the process by complex formation with Zn(II). Moreover, in this way the deposited ZnO can adhere very strongly to the surface of the virion.

While the ELD of metals on TMV (and on other surfaces) can be sensitized by a large variety of noble metals (Ag, Au, Pd, Pt), the catalytic action of Pd appears to be unique for ZnO deposition: TMV particles were also sensitized with an aqueous solution of Pt(II) and then treated with the ZnO ELD bath. No ZnO coating was found, but ZnO agglomerates were observed in the reaction solution (white precipitate). Obviously, the catalytic activity depends on the exact chemical nature of the metal. In fact, Pd is more active for DMAB reduction (higher rate) than Pt [16], which strongly supports the chemical reaction model we present in the following.

3. Results and discussion

3.1. Electrochemical mechanisms

First we concentrate on the formation of ZnO, which requires – at least locally – an increase in pH to create hydroxide. Tests for ELD of ZnO on palladium-sensitized glass surfaces indeed indicated that the pH of the solution increases during the process. The generated hydroxide ions react with the Zn(II) ions present in the solution (Zn(II) cannot be reduced to its metallic state by DMAB), causing ZnO formation (reactions (1) and (2)).

$$Zn^{2+} + 2OH^- \rightarrow Zn(OH)_2 \tag{1}$$

$$Zn(OH)_2 \rightarrow ZnO + H_2O \tag{2}$$

We note that the surfaces of as-deposited ZnO quantum dots are passivated by a thin layer of $Zn(OH)_2$, thus, "ZnO" particles in fact consist of a $ZnO/Zn(OH)_2$ core–shell structure [17]. In order to convert all $Zn(OH)_2$ to ZnO, annealing is required.

Like on any substrate surface, the observed selective ZnO deposition on the surface of TMV requires that palladium ions adhere before the actual deposition starts, e.g. by forming complexes with functional groups of the amino acids on the exterior surface of the virion. A possible route is complexation: Apart from the C terminal carboxylate, Asp64 and Asp66 can offer carboxylate groups, and
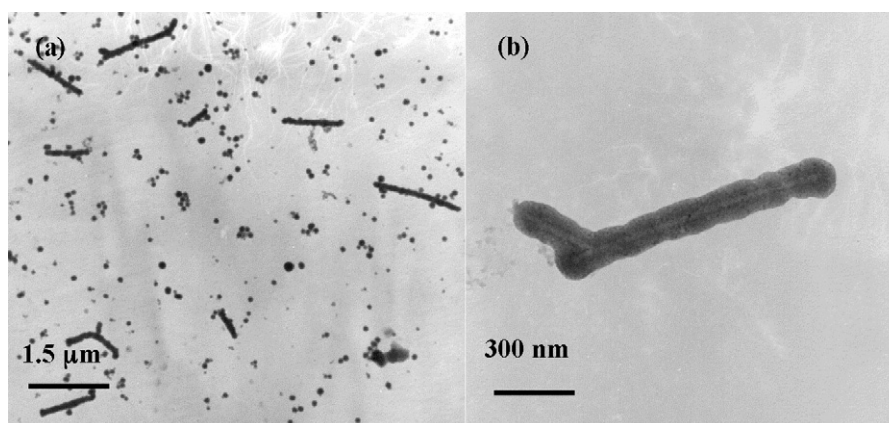
Fig. 1. TEM micrograph of ZnO deposited on the surface of TMV particles. (a) Large area imaging. The diameter of the ZnO rods is in between 100 and 150 nm and the length of the structures reaches several micrometers, depending on the number of end-to-end assembled virions. (b) Imaging of a single ZnO rod. TMV particles (light grey) can be observed in the center of the ZnO rod (dark grey).

Arg61 and Arg141 provide amines, both possible ligands for Pd(II). The ions are reduced by DMAB, as soon as the ELD bath is added, and coalesce to particles. The mechanism of the ELD of ZnO on these catalytic centers is not quite clear. Certainly, NO_3^- is required [13], and DMAB reduces it to various products (see Eqs. (3) to (5)).

$$NO_3^- + H_2O + 2e^- \rightarrow NO_2^- + 2OH^- \quad (3)$$

$$NO_2^- + H_2O + e^- \rightarrow NO + 2OH^- \quad (4)$$

$$NO_3^- + 2H_2O + 3e^- \rightarrow NO + 4OH^- \quad (5)$$
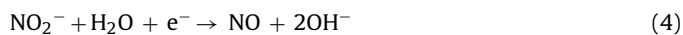
The overall reaction is best formulated with species stable at neutral pH, yielding NO_2^- or NO (Eqs. (6) and (7)).

$$4(CH_3)_2NHBH_3 + 12NO_3^-$$
$$\rightarrow HB_4O_7^- + 4(CH_3)_2NH_2^+ + 2H_2O + 12NO_2^- + 3OH^- \quad (6)$$

$$4(CH_3)_2NHBH_3 + 8NO_3^- + 2H_2O$$
$$\rightarrow HB_4O_7^- + 4(CH_3)_2NH_2^+ + 8NO + 11OH^- \quad (7)$$
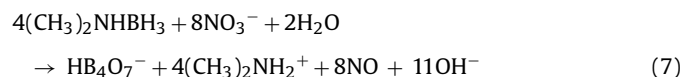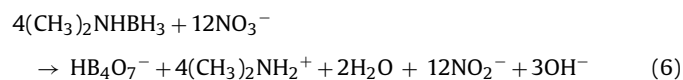
Hence hydroxide is generated by the reduction of nitrate, which is not possible when boric acid H_3BO_3 instead of $HB_4O_7^-$ and $(CH_3)_2NH$ instead of $(CH_3)_2NH_2^+$ are assumed to be dominant [18]. In other words, formulating the reaction with boric acid cannot result in production of hydroxide:

$$(CH_3)_2NHBH_3 + 3NO_3^- \rightarrow H_3BO_3 + (CH_3)_2NH + 3NO_2^- \quad (8)$$
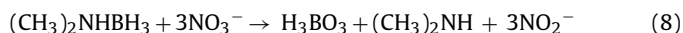
Let us note that after (7) further reduction of NO might ensue; since no formation of N_2 or N_2O has been detected on a variety of metal surfaces, negative oxidation numbers of nitrogen, such as in NH_3 or NH_2OH, might be attained [19]. However, the mechanism of nitrate reduction on various catalytic surfaces is well known, and the rate-determining step is the conversion to nitrite, generating hydroxide (3). In this step, the palladium can catalyze the reduction [19]. The fate of the nitrite ion is determined by its high reactivity on transition-metal surfaces: It produces chemisorbed NO [20]. Therefore, it is generally assumed that reaction (3) is quickly followed by reaction (4) [19].

In order to confirm the presence of nitrite during the reduction of nitrate, a standard nitrate test was used (see supporting information). Nitrate-containing solutions were treated with surplus metallic zinc (to reduce all nitrate). After 30 min, the produced nitrite was treated with sulfanilic acid and 1-naphtylamine to generate a dye with an absorption maximum at ∼520 nm [21]. Aliquots taken at the beginning and after 30 min of the deposition show that there is no absorption increase during 30 min (white ZnO precipitate was observed). After 12 h, a similar experiment was carried out. An increase in the absorbance of the produced dye suggests that only at the later stage of the ZnO deposition, nitrite was present in the deposition solution (Fig. 2). At this stage, the catalyst surfaces might be covered with ZnO; hence the conversion of NO_2^- to NO could be minimized, thereby increasing the concentration of the nitrite [20].

It is clear that at the beginning of ZnO deposition no nitrite is present; therefore reaction (7) is preferred over (6). This also correlates with other experimental observations [19,20]. Nonetheless, Izaki and co-workers suggested that the final product of nitrate reduction is nitrite, which we can exclude at least for the beginning of the ZnO deposition. Only during the later stages nitrite is dominant (reaction (6)).

Since ZnO does not show catalytic properties, in any case the reducing agent together with the nitrate ions must be in contact with the catalytic surface (or in direct proximity). Once nitrite is produced, it can be reduced further on transition-metal surfaces [20], which explains why no nitrite is present at the late stages of the ELD of ZnO. Based on this and on our experimental observations, three different ZnO deposition mechanisms are possible
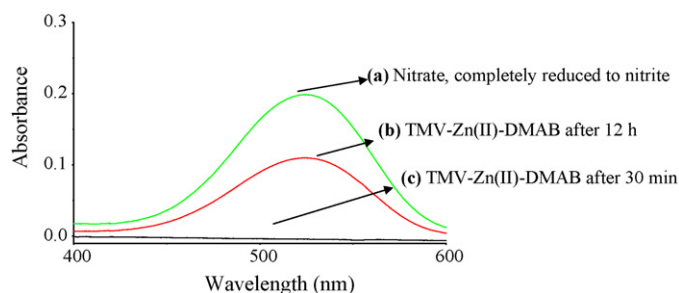
Fig. 2. UV–vis spectra of aliquots taken from solutions or suspensions, each with 0.8 mM nitrate. The aliquots were mixed with sulfanilic acid and 1-naphtylamine to convert the produced nitrite into a strongly light-absorbing azo compound. (a) Standard nitrate solution after complete reduction with zinc; (b) TMV-ZnO solution 30 min after the initiation of the deposition, no nitrite is detected; (c) TMV-ZnO solution 12 h after initiation, nitrite is present.

(Scheme 1). In Scheme 1a, catalyst particles are assumed to be constantly present on the growing ZnO layer. Therefore, hydroxide and Zn(II) have to be continuously supplied without covering the particles, which would require palladium diffusion, a rather slow process, or detachment of the palladium particles. Such a mechanism is much more plausible for gold nanoparticle-catalyzed ZnO nanorod fabrication, which is carried out at elevated temperatures, and includes vapor transport and condensation [2]. A second possibility is illustrated in Scheme 1b: Catalyst particles are buried within the ZnO layer, but remain attached to the virion surface. In fact, palladium particles of up to 8 nm size are observed after the reduction of Pd(II) on TMV [6]. Saito et al. found palladium particles on palladium-sensitized SiO_2, below, but not in a ZnO layer grown from $Zn(NO_3)_2$ and DMAB [14]. The interpretation is not trivial, because the catalytic properties of the palladium have to be somehow transferred to ZnO to sustain constant growth. Therefore, we propose that the mechanism in Scheme 1c operates, namely a combination of both mechanisms 1a and 1b, the latter only operating at the first stages of the reaction. In this way, the growth is first very fast, but most catalytic centers are inactivated by ZnO, and the few centers that detach from the virion support a further slow growth, and slowly destroy the produced nitrite. The granularity of the ZnO structure might arise from the inhomogeneous distribution of the catalyst particles on the TMV surface, and especially from that of the detached palladium.

3.2. Nanoscale analysis

The chemical composition of the deposited material was revealed by energy filtering TEM (EFTEM) [7]. Fig. 3 shows electron energy loss spectra (EELS) from the zinc $L_{2,3}$ and the oxygen K edges, which compare well with those obtained from ZnO on silicon oxide [22]. The carbon peak arises from the TMV particles, and also from the TEM grid support. We were unable to detect palladium signals, hence its content is below the detection limit (some %). We can expect minimal amounts of boron from borane (well below 0.1% [18]), which would suggest similar levels of nitrogen (from dimethylamine). In contrast, the zinc and oxygen peaks are clearly resolved. While the oxygen peak is well comparable to standard spectra, the zinc edge is rather broad, as also found for zinc oxide powder and nanoparticles [22]. The two L edges of zinc are closely spaced: At 1023 eV the spectrum shows a steep step, while the edge at 1040 eV is less clear, as well known for ZnO nanoparticles [22]. However, zinc and oxygen maps of the produced ZnO rod were obtained in a straightforward manner by the common three-window technique. Fig. 4a shows a TEM image of a rod synthesized from the Zn(II) containing ELD bath. The rod has a length of 900 nm and a diameter of 120 nm, likely containing three TMV particles in
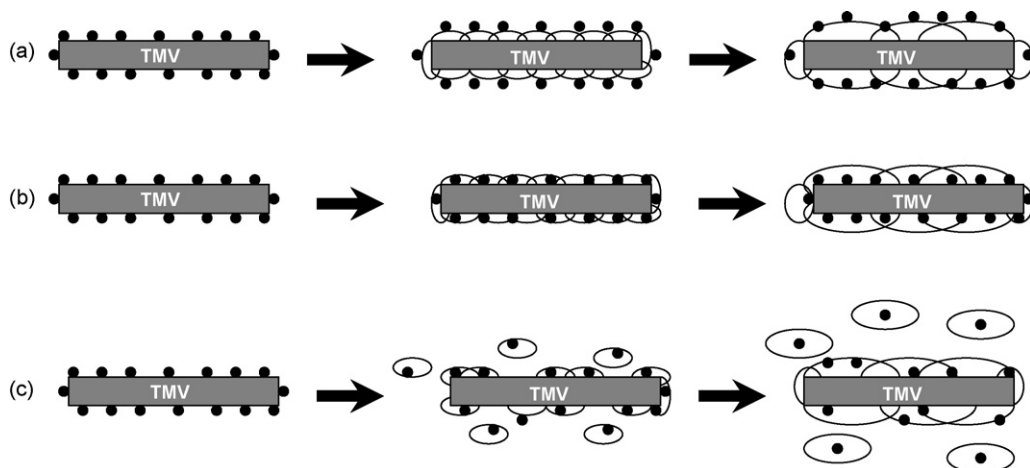
Scheme 1. Possible mechanisms for electroless deposition of ZnO on TMV. (a) Palladium particles (larger than 1 nm) are produced on TMV. Hydroxide is produced only on the palladium. Zn(II) attaches to the TMV surface, and ZnO grows underneath the palladium particles. (b) The palladium particles remain on the surface of the virion during ZnO growth. (c) Only a part of the palladium particles remain on the virion, the other part detaches and produces ZnO particles in the suspension. Particles can reattach to the growing ZnO layer on the virion.
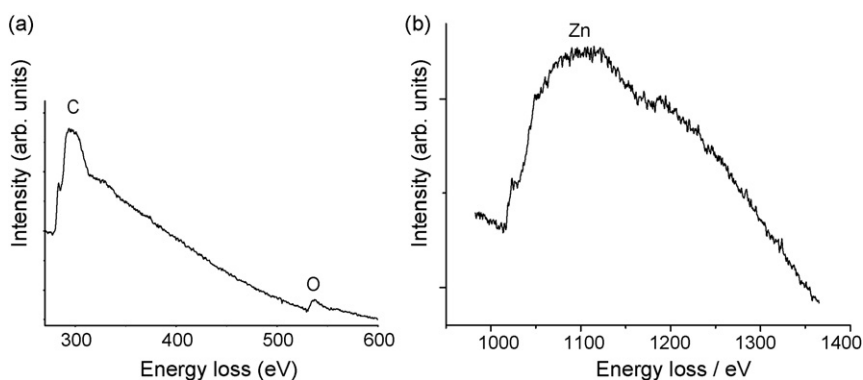
Fig. 3. Electron energy loss spectra of carbon, oxygen, and zinc recorded in the TEM. The material was synthesized from TMV-Zn(II)-DMAB and deposited on a Cu-TEM grid surface (see Fig. 1). (a) Carbon K-edge at 284 eV, oxygen K-edge at 532 eV; (b) zinc $L_{2,3}$-edge at 1020 and 1043 eV.
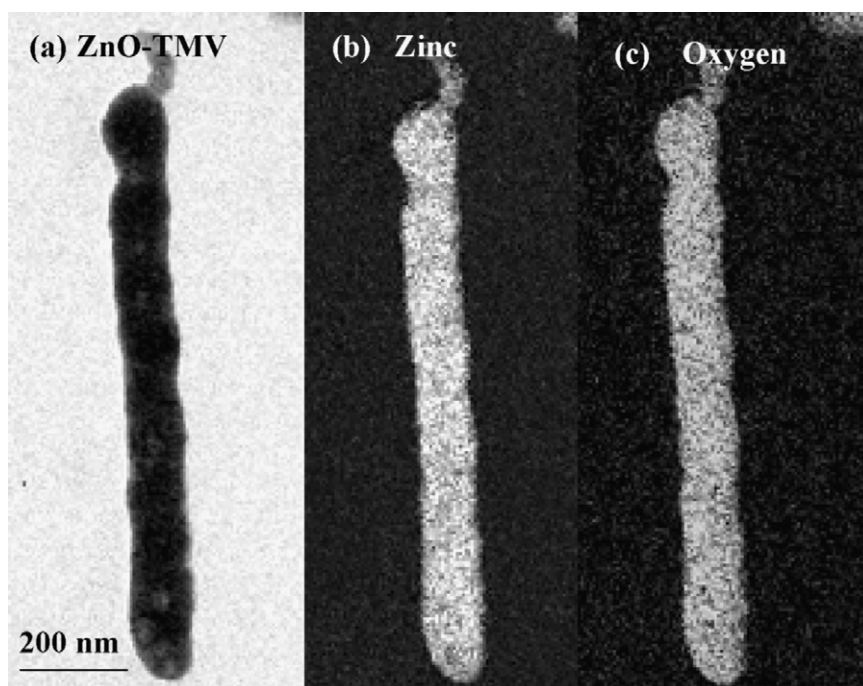
Fig. 4. Elemental maps of a ZnO rod, based on energy filtering TEM (see Fig. 3). (a) TEM micrograph of ZnO deposited on the surface of TMV particles. The length of the rod corresponds to three virions (~900 nm). (b) Zinc map (zinc $L_{2,3}$ edges at 1020 and 1043 eV), (c) oxygen map of the rod (oxygen K-edge at 532 eV).

end-to-end assembly. The particle (~100 nm in length) attached to the upper end of the rod in Fig. 4a could be the RNA of a partially uncoated TMV coated with the deposited ZnO. Note that the ZnO rod in Fig. 4a is not completely smooth, but granular in shape. This is also supported by the oxygen and zinc elemental maps, which reproduce the bright-field TEM image to nearly all details. The granular shape can be interpreted as originating from the variable deposition rates of ZnO at different locations of the virions. As discussed above, the amount of catalyst (palladium) attached to the surface of the virion has a big influence; although many catalytic nuclei may be present, it appears as if only very few, one or two per 50 nm TMV length, are so active that the material growth wins over all other nuclei.

We did not yet investigate the crystalline structure of the deposit; however, X-ray diffraction of bulk samples of electrolessly deposited ZnO produced under very similar conditions (no heating) shows the wurtzite structure [18]. It is likely that our ZnO grains, which are not true nanoscale deposits, but contain hundreds of atomic planes, have the same structure since bulk properties are expected for such large structures. The optical properties discussed in the following section point to the same conclusion.

3.3. Cathodoluminescence

Recently, ZnO was selectively deposited from $Zn(NO_3)_2$ and DMAB on a pattern of catalytically sensitized regions on SiO_2 surfaces. The pattern was analyzed by cathodoluminescence (CL), which proved the desired UV emission [14]. In our case, the luminescence from the ZnO rods is restricted to the coated virions, hence to nanoscale areas. CL is here one of the few suitable methods to obtain data on the optical properties. We employed oxidized silicon substrates, cooled to 10 K in a CL scanning electron microscope (SEM) [23]. Fig. 5a shows a SEM micrograph of ZnO-coated TMV particles. A CL spectrum from the region in Fig. 5a, in which two TMV-ZnO rods form a cross, is shown in Fig. 5b. The emission around 3.36 eV is due to donor-bound exciton recombination in hexagonal bulk-like ZnO, consistent with literature values for bulk ZnO [24]. This dominant CL peak is relatively narrow (~1.5 meV), indicating quite good crystalline quality. The emission energy is exactly the same as in bulk material, thus no quantization effect due to the size of the rods occurs. The broader band around 3.31 eV is characteristic for emission from defects related to stacking faults [25,26].

In Fig. 5a, one of the ZnO rods has no contact to the substrate material, which we consider as a hint that the silicon/SiO₂ substrate causes quenching of the CL intensity. In fact, on all other sites we observed very fast quenching of the CL intensity on a time scale of a few seconds. Further experiments were carried out on a carbon coated copper TEM grid. In this case, CL signals were detected only from material adsorbed on the copper parts of the grid, while on the carbon-only-coated surface no CL was found. We propose that carbon, different from copper, quenches the CL.

4. Conclusions

We have developed an elegant, fast, and simple synthesis of ZnO grown from aqueous solutions on the surface of suspended TMV particles. Spectrophotometric analysis of the ZnO deposition mechanism indicated that nitrite, considered to be produced in the solution, is not present at the beginning of the deposition reaction (after 30 min). Hence nitrate, which is an important species in the deposition of ZnO, must be further reduced to other species like NO. Three possible ZnO growth mechanisms on the surface of the virions were discussed in the light of the experimental observations. In contrast to other mineralization reactions [6,7], ZnO can bind to functional groups on the surface of the virion, based on complex formation with Zn(II). As a result, ZnO adheres very strongly. TEM experiments show that the material deposited on the surface of the TMV particles from the $Zn(NO_3)_2$/DMAB bath includes zinc and oxygen. Both zinc and oxygen elemental maps obtained by EFTEM reproduce the bright-field TEM images. Thus, TMV particles are mineralized with ZnO. CL measurements of the deposited material show ultraviolet emission with a photon energy of around 3.36 eV, which corresponds to the band gap of hexagonal bulk ZnO.

Fig. 5. SEM micrograph and cathodoluminescence (CL) spectrum recorded at 10 K from ZnO-covered TMV particles. (a) ZnO-coated TMV particles adsorbed on an oxidized silicon wafer. The rectangular box indicates the region where CL was excited. (b) Corresponding CL spectrum. BSF marks emissions from basal stacking faults, and D^0X is a neutral donor bound exciton emission either linked to the A or B valence band (lower index).

References

[1] C.M. Lieber, Sol. State Commun. 107 (1998) 607.
[2] M.H. Huang, S. Mao, H. Feick, H.Q. Yan, Y.Y. Wu, H. Kind, E. Weber, R. Russo, P.D. Yang, Science 292 (2001) 1897.
[3] K.A. Alim, V.A. Fonoberov, A.A. Balandin, Appl. Phys. Lett. 86 (2005) 053103.
[4] P. Gerstel, R.C. Hoffmann, P. Lipowsky, L.P.H. Jeurgens, J. Bill, F. Aldinger, Chem. Mater. 18 (2006) 179.
[5] W. Shenton, T. Douglas, M. Young, G. Stubbs, S. Mann, Adv. Mater. 11 (1999) 253.
[6] M. Knez, A.M. Bittner, F. Boes, C. Wege, H. Jeske, E. Maiβ, K. Kern, Nano Lett. 3 (2003) 1079.
[7] S. Balci, A.M. Bittner, K. Hahn, C. Scheu, M. Knez, A. Kadri, C. Wege, H. Jeske, K. Kern, Electrochim. Acta 51 (2006) 6251.
[8] M. Demir, M.H.B. Stowell, Nanotechnology 13 (2003) 541.
[9] T.L. Schlick, Z. Ding, E.W. Kovacs, M.B. Francis, J. Am. Chem. Soc. 127 (2005) 3718.

[10] K. Namba, R. Pattanayek, G. Stubbs, J. Mol. Biol. 208 (1998) 307.
[11] A. Nedoluzhko, T. Douglas, J. Inorg. Biochem. 84 (2001) 233.
[12] M. Izaki, T. Omi, Appl. Phys. Lett. 68 (1996) 2439.
[13] M. Izaki, T. Omi, J. Electrochem. Soc. 144 (1997) L3.
[14] N. Saito, H. Haneda, T. Sekiguchi, N. Ohashi, I. Sakaguchi, K. Koumoto, Adv. Mater. 14 (2002) 418.
[15] M. Schlesinger, M. Paunovic, Modern Electroplating, John Wiley & Sons, New York, 2000.
[16] I. Ohno, O. Wakabayashi, S. Haruyama, J. Electrochem. Soc. 132 (1985) 2323.
[17] H. Zhou, H. Alves, D.M. Hofmann, W. Kriegseis, B.K. Meyer, G. Kaczmarczyk, A. Hoffmann, Appl. Phys. Lett. 80 (2002) 210.
[18] M. Izaki, J. Katayama, J. Electrochem. Soc. 147 (2000) 210.
[19] G.E. Dima, A.C.A. De Vooys, M.T.M. Koper, J. Electroanal. Chem. 554 (2003) 15.
[20] A. Rodes, R. Gomez, J.M. Orts, J.M. Feliu, J.M. Perez, A. Aldaz, Langmuir 11 (1995) 3549.
[21] J.S. Fritz, G.H. Schenk, Quantitative Analytical Chemistry, Allyn and Bacon, Boston, 1974.
[22] K. Giannakopoulos, N. Boukos, A. Travlos, T. Monteiro, M.J. Soares, M. Peres, A. Neves, M.C. Carmo, Appl. Phys. A 88 (2007) 41.
[23] M. Schirra, A. Reiser, G. M. Prinz, A. Ladenburger, K. Thonke, R. Sauer, J. Appl. Phys. 101 (2007) 113509, and Virtual Journal of Nanoscale Science and Technology, Vol. June 18, 2007.
[24] B.K. Meyer, H. Alves, D.M. Hofmann, W. Kriegseis, D. Forster, F. Bertram, J. Christen, A. Hoffmann, M. Strassburg, M. Dworzak, U. Haboeck, A.V. Rodina, Phys. Stat. Sol. 241 (2004) 231.
[25] M. Schirra, R. Schneider, A. Reiser, G.M. Prinz, M. Feneberg, J. Biskupek, U. Kaiser, C.E. Krill, K. Thonke, R. Sauer, Phys. Rev. B 77 (2008) 125215.
[26] A. Reiser, A. Ladenburger, G.M. Prinz, M. Schirra, M. Feneberg, A. Langlois, R. Enchelmaier, Y. Li, R. Sauer, K. Thonke, J. Appl. Phys. 101 (2007) 054319.